Available online at www.sciencedirect.com

jmr&t Journal of Materials Research and Technology

journal homepage: www.elsevier.com/locate/jmrt

Original Article

Indentation-induced cracking behavior of a $Cu(In,Ga)Se_2$ films on Mo substrate

Dayoung Yoo [a], *Mao Zhang* [a], *Changsoon Choi* [b], *Byungha Shin* [c], *Yoon-Hwae Hwang* [a,e], *Yangdo Kim* [d,**], *Dongyun Lee* [a,e,*]

[a] *Department of Nano Fusion Technology, Pusan National University, Busan 46241, Republic of Korea*
[b] *Department of Energy and Materials Engineering, Dongguk University-Seoul, Seoul 04620, Republic of Korea*
[c] *Department of Materials Science and Engineering, Korea Advanced Institute of Science and Technology, Daejeon 34141, Republic of Korea*
[d] *School of Materials Science and Engineering, Pusan National University, Busan 46241, Republic of Korea*
[e] *Department of Nanoenergy Engineering, Pusan National University, Busan 46241, Republic of Korea*

ARTICLE INFO

Article history:
Received 27 January 2021
Accepted 22 May 2021
Available online 29 May 2021

Keywords:
CIGS compound
Brittle fracture
Intergranular fracture
Nanoindentation

ABSTRACT

$Cu(In,Ga)Se_2$ (CIGS) light absorption films were synthesized by co-sputtering method on Mo/soda-lime glass, and the mechanical behavior of the films was investigated by nano-indentation. The Young's modulus and hardness of the films were approximately 88.5 ± 2.2 and 5.89 ± 0.23 GPa, respectively. The comparison graph of indentation load–displacement curve with the curve based on the theoretical elastic films, while considering the curvature of the indenter tip, revealed that cracks initiated in the CIGS films at approximately 25 mN indentation load. The transmission electron microscopy (TEM) analysis revealed that most of the cracks exhibited intergranular fracture, and the fracture toughness of the films was ~0.22 MPa$\sqrt{m}$, which is greater than the brittleness of soda-lime glass. Both Palmqvist radial and lateral cracks are observed. Results also reveal that the indentation pressure caused grain subdivision (before cracking initiated), and indentation stress may be absorbed by relatively less dense microstructures of the films.

1. Introduction

Film-based cells have attracted significant attention for the application in photovoltaic devices because they can be applied to low-cost roll-to-roll processes and can attain well-established efficiencies; for example, $Cu(In,Ga)Se_2$ (CIGS) absorber material-based film photovoltaics achieved an efficiency of approximately 20% even in modules [1,2]. Several studies have been carried out on flexible solar cells using CIGS light absorption layer materials, and the mechanical properties of CIGS and substrate materials have also been investigated. For example, Gerthoffer et al. [1] reported that the elastic modulus and hardness of CIGS light absorption layer material are 68 ± 2 GPa and 3.0 ± 0.1 GPa, respectively. In addition, Lai et al. [3] reported that the elastic modulus and hardness of CIGS

* Corresponding author.
** Corresponding author.
E-mail addresses: yangdo@pusan.ac.kr (Y. Kim), dlee@pusan.ac.kr (D. Lee).
https://doi.org/10.1016/j.jmrt.2021.05.059

light absorption layer material are 83 and 4.75 GPa, respectively. The differences in the reported values can be attributed to the differences in the microstructures of the films depending on the types of substrates and manufacturing methods.

There are several studies on elasticity and strength, but not many studies on the fracture/cracking phenomenon of CIGS compound films. Research on the fracture toughness of CIGS films is inadequate, and studies are needed in terms of reliability and application of flexible devices for CIGS films. It is thought that one of the most suitable methods for measuring the fracture toughness of the deposited film is to use indentation, and it is known that the measurement using a Berkovich indenter is more accurate [4]. Nanoindentation method is a particularly practical tool to study the fracture behavior of thin films with brittleness and was used in this study to investigate the cracking behavior of CIGS films. To accurately define the shape of the indenter tip, we referred to Bei et al. [5] and Morris et al. [6] research works. Based on this, the actual experimental results and theoretical values were compared and analyzed. The proposed study aims to investigate the mechanical properties and fracture behavior of compound films and to discuss the improvement of the resistance of the compound films to cracking.

2. Experimental procedure

2.1. *Fabrication of Cu(In,Ga)Se_2 (CIGS) films*

In this study, CIGS films were grown on a Mo-coated soda-lime substrate using a co-sputtering system. Mo layer was coated by DC sputtering on soda lime glass [7]. For CIGS films, In and Ga were first co-deposited on the Mo layer, followed by Cu; this procedure was repeated 10 times to achieve a desired film thickness of 1.5–1.7 μm. Sputtering targets were used high purity elements, ~99.999% (MARU L&C, Korea). During the deposition, the substrate temperature was maintained at 350 °C at a constant Ar working pressure of 3 mTorr. Subsequently, the films were annealed at 400 °C under selenium (Se) atmosphere. After selenization, the sulfurization process was carried out to create a band gap opening at the CIGS surface. X-ray diffraction (XRD) and compositional analysis by energy dispersive spectroscopy (EDS) were used to observe crystal structures and compositional distribution which are presented in supporting information. The EDS element mapping results show that S and Se are evenly distributed across the entire thickness. The final composition of bulk CIGS was determined to be $Cu_{0.9}(In_{0.7}Ga_{0.3})Se_2$, which corresponded to a band gap of approximately 1.17 eV. The bandgap of CIGS was extracted by an external quantum efficiency (EQE) measurement (QEX7 solar cell spectral response/QE/IPCE measurement system, PV measurement) [8,9]. All the CIGS absorbers used in this study were grown in the same batch to eliminate possible run-to-run fluctuations.

2.2. *Measurement of mechanical properties by nanoindentation*

The mechanical properties of fabricated CIGS films were measured using a nanoindentation system (Nanoindenter® G200, KLA Co. USA), and the specifications of the system were as follows: maximum load of 500 mN, load resolution of 50 nN, load frame stiffness of ~5 × 10^6 N/m, maximum indentation depth of 500 μm, and depth resolution of 0.01 nm [10]. A Berkovich indenter (centerline-to-face angle of 65.3°), which is a three-sided pyramid diamond tip with the same area-to-depth ratio as a traditional Vickers indenter, was used for this study. The nanoindentation experiments were carried out 30 times and the mechanical properties was calculated using the mean value of the experiments [11]. The Berkovich diamond indenter, given additional harmonic movements with an amplitude of 2 nm and frequency of 45 Hz following the continuous stiffness measurement (CSM) technique [12], was pressed into the specimen to up to 500 and 1000 nm at a strain rate of 0.01 s^{-1}. Each test was performed when the thermal drift dropped to 0.01 nm/s.

The Lawn-Evans-Marshall (LEM) model is a method commonly used to measure fracture toughness using an indenter and is as shown in the following Eq. (1) [13–17], and Ouchterlony standardized K_c for Berkovich indenter [4];

$$K_c = \alpha\left(\frac{E}{H}\right)^{1/2} \times \left(\frac{P_{max}}{C^{3/2}}\right) \quad (1)$$

$$K_c = x_b\left(\frac{a}{l}\right)^{1/2}\left(\frac{E}{H}\right)^{2/3} \times \left(\frac{P_{max}}{C^{3/2}}\right) \quad (2)$$

where P_{max} is the maximum indentation load, E and H are the Young's modulus and hardness of the specimen, respectively, c is the crack length from the center of indentation, l and a are defined in Fig. 1 (b), and α and x_b are empirical constants that depend on the geometry of the indenter tips ($\alpha = 0.015$ for a Vickers tip, and $x_b = 0.016$ for a Berkovich tip). These are used under long cracks ($l/a>>1$).

The Young's modulus (E) and hardness (H) were obtained from the indentation curves [18,19]. E and H were estimated from the indentation load (P), indentation depth (h), and time using the Sneddon stiffness equation [20], which is suitable for conical indenter tips. Using different shape indenter tips, the equation is multiplied by a correction factor (β):

$$S = \frac{dp}{dh} = \frac{2}{\sqrt{\pi}} E_{eff} r\sqrt{A} \quad (3)$$

$$E_{eff} = \frac{1}{\beta}\frac{\sqrt{\pi}}{2}\frac{S}{\sqrt{A}} \quad (4)$$

where S is the stiffness, which is the gradient of curves at the maximum indentation load. The β for Berkovich tip is 1.034. E_{eff} is related to the Young's modulus of specimen (E_s), Young's modulus of indenter tip (E_i), and Young's modulus of the specimen can be obtained using the following equation:

$$\frac{1}{E_{eff}} = \frac{(1-\nu_s^2)}{E_s} + \frac{(1-\nu_i^2)}{E_i} \quad (5)$$

where ν_s is Poisson's ratio of the specimen and ν_i is Poisson's ratio of the indenter tip. E_i and ν_i are 1141 GPa and 0.07, respectively.

Projected area A can be obtained from the experimental function of contact depth h_c; h_c expresses the difference

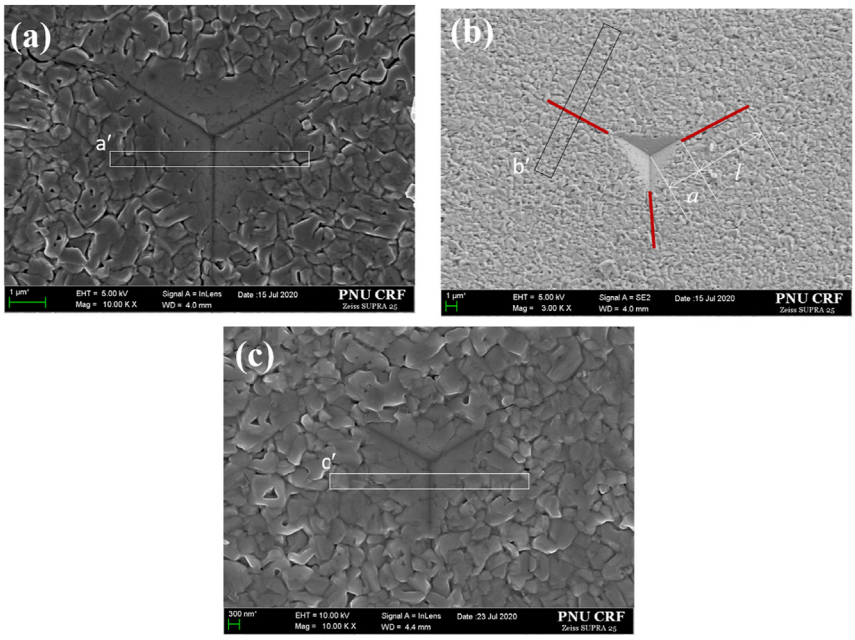

Fig. 1 – (a) Nanoindentation experiments performed on the CIGS films synthesized by co-sputtering method. The formation of cracks in the filma at the edge of the indenter can be observed. (b) and (c) SEM images of the CIGS filma at depth of 1000 nm and 500 nm, respectively.

between the total displacement (h_{max}), and elastic deformation (h_s) in the schematic in [19].

$$h_c = h_{max} \times h_s = h_{max} - \varepsilon \frac{P}{S} \quad (6)$$

The shape coefficient (ε) of the three-sided pyramid indenter tip (Berkovich, Cube-corner) was 0.75 [21]. For more accurate characterization, the analysis of the geometry of the indenter tip was obtained from the study of Bei et al. [5] and Morris et al. [6], and the radius of the tip was calculated to be relatively sharp at approximately 54 nm.

The microstructural deformation, which occurred in the sample during the indentation process, was observed by scanning electron microscopy (SEM) and transmission electron microscopy (TEM). The TEM samples were obtained using focused ion beam (FIB).

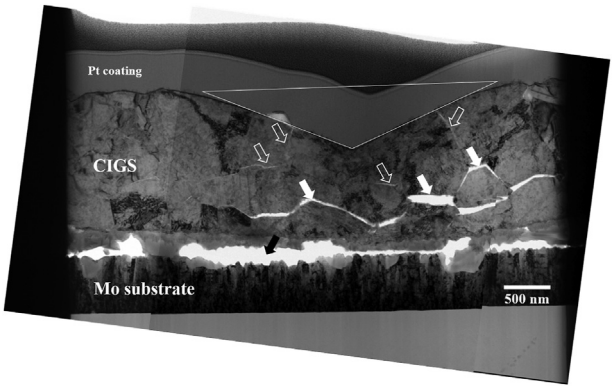

Fig. 2 – TEM images of the CIGS films after the nanoindentation tests at a depth of 1000 nm – cracks. Mostly, intergranular cracks can be observed near the interface between the film and substrate.

3. Results and discussion

The SEM analysis results of the CIGS films after the nanoindentation experiment are shown in Fig. 1. Crystal structures analysis by XRD, cross-sectional SEM images, and composition distribution analysis in film thickness by EDS are shown in Fig. S1. Figure 1a and b shows the SEM images of the indentation on the CIGS films pressed to a depth of 1000 nm, and Fig. 1c shows the indentation on the CIGS films pressed to a depth of 500 nm. The thickness of CIGS films was approximately 1650 nm, indicating that the films were pressed to a depth corresponding to approximately 60% and 30% of the thickness of the films at 1000 and 500 nm, respectively. This is a rather deep indentation depth to measure the mechanical properties of the films without the effect of the substrate. As will be explained later, in general, in the case of the films placed on a rigid substrate (Mo), the modulus and hardness increase due to the influence of the substrate as the indentation depth increases, but such a phenomenon was not seen in this study. This is judged by the influence of the microstructure. Nevertheless, efforts were made to measure the properties of the films, while minimizing the effect of substrate using the CSM method.

The rectangles in Fig. 1 show the locations where the samples for the TEM analysis were cut with FIB (Figs. 2–4). The shape of TEM sample cut with FIB is shown in Fig. S2. The SEM image (SE2 image) in Fig. 1b was taken at low magnification to reveal the length of the crack formed at the edge of the Berkovich indenter tip. The red line in Fig. 1b represents the length of the cracks. The average length of the crack, l, was approximately

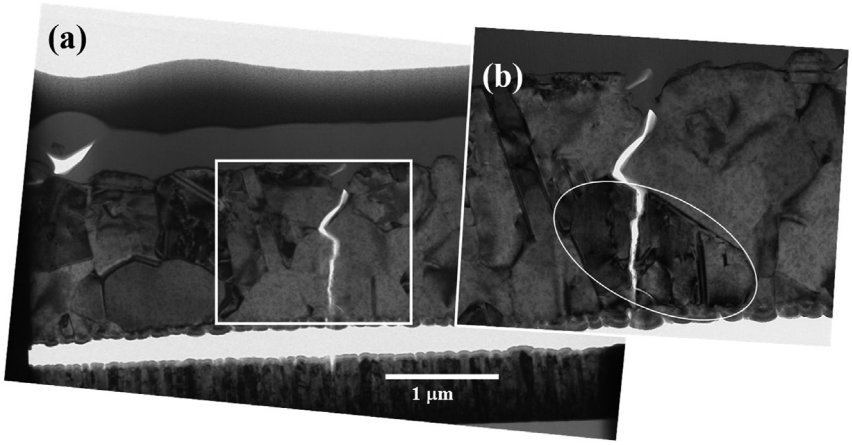

Fig. 3 – TEM images of the CIGS films after the nanoindentation tests (a) at a depth of 1000 nm – cracks; (b) enlarged micrograph of the square in (a) – trans-granular crack.

5.20 ± 1.77 μm. On the other hand, as shown in Fig. 1c, cracks are hardly observed around the indentation because no force was applied to the critical load that generates cracks.

The TEM analysis results of the rectangular part of Fig. 1 are shown in Fig. 2. The part indicated by the black arrow at the bottom of the image is a crack generated when the boundary between the Mo substrate and the CIGS films fell off during the fabrication of the TEM specimen. The falling off of the $MoSe_2$ layer [22] formed between the Mo substrate and CIGS films during the FIB process induced the generation of crack in the films. In addition, relatively large cracks were observed at the bottom of the films, as indicated by the closed white arrows. It is unclear if the large cracks were more open during specimen preparation. However, as indicated by the open white arrows on the top of the films and the closed white arrows at the bottom, cracks were formed not only throughout the thickness of the films, but also parallel to the films. In general, we may adopt typical crack patterns to understand how cracks initiate and propagate. From the results of Figs. 1 and 2, it can be seen that both Palmqvist radial cracks and lateral cracks are observed. Palmqvist radial cracks are generally occurred in high load, which is related to plastic deformation of the films [15]. It is known that radial cracks are formed by defects at the boundary of the deformation region and are induced by a residual stress field resulting from the deformation mismatch of the plastic deformation zone on the rigid substrate; white arrows may indicate cracks by the defects at the grainboundary and plastic zone mismatch [23]. It is also known that lateral cracks generated beneath the plastic deformation zone along with surface [24]; white closed-arrows indicate lateral cracks underneath of indents parallel to the surface. In addition, it is generally known that lateral cracking occurs during the unload cycle, but it was difficult to confirm in this study [23,24].

According to the TEM analyses, the diameter of the grains was approximately 500 nm to 1 μm, and most of the cracks were intergranular fractures. And, the grain boundaries were not clearly visible just below the indentation, and the reason for this will be discussed in detail in association with Figs. 4 and 5. Of course, as shown in Fig. 3, transgranular fractures are also formed. Figure 3 shows a high-resolution image of the TEM specimen in the square of Fig. 1b. Figure 3b shows an enlarged view of the square in Fig. 3a, and the image was obtained by observing the specimen from a slightly different angle. Figure 3b confirms the presence of transgranular fracture in the specimen. It can be observed that the white ellipse in Fig. 3b is a crystal and the crack propagates inside the crystal.

The indentation depths on the films after the elastic recovery of the film at the 1000 and 500 nm depths were estimated using the TEM images, as shown in Figs. 2 and 4, as approximately 685 nm ($h_c = 685$ nm) and 381 nm ($h_c = 381$ nm), respectively. These results may show slight deviations because the TEM specimen may not perfectly obtain the point of pyramid of the indenter tip. However, the values were close to the final depths measured from the load–displacement curves in Figs. 5 and S3.

Presumably, cracks started to propagate at the edges of the indent tip on the CIGS at approximately 25 mN because curvature of loading curves is changed, as shown in Fig. 5. The fracture toughness, K_C, of the CIGS was calculated using Eq. (2). Based on the results, the fracture toughness was approximately 0.22 MPa$\sqrt{m}$ with large diversity depend upon measurement of crack length up to 0.45 MPa$\sqrt{m}$, which is similar to those of silicon and soda-lime glass [25] and intermetallic compound [26]. Fig. S4 shows the SEM images of the indentation pressed by several hundred mN for indenting position calibration. The brittleness of the films can be clearly observed in the image. The peeling of the layer between the films and substrate can also be observed. In general, when a film formed on a hard substrate is tested by the CSM method, the modulus and hardness of the films increase due to the influence of the substrate according to the indentation depth. However, such an effect was not observed in this study (refer to Fig. S3). The substrate effect cannot be observed. Since the density of the films is relatively low, it is estimated that it is less affected by the substrate than the dense films because it has the capacity to absorb the energy caused by indentation. However, when the pressure further increases, the plastic deformation zone affects the substrate, and lateral cracks appear to occur along the substrate. As the pressure increases, there is no room for

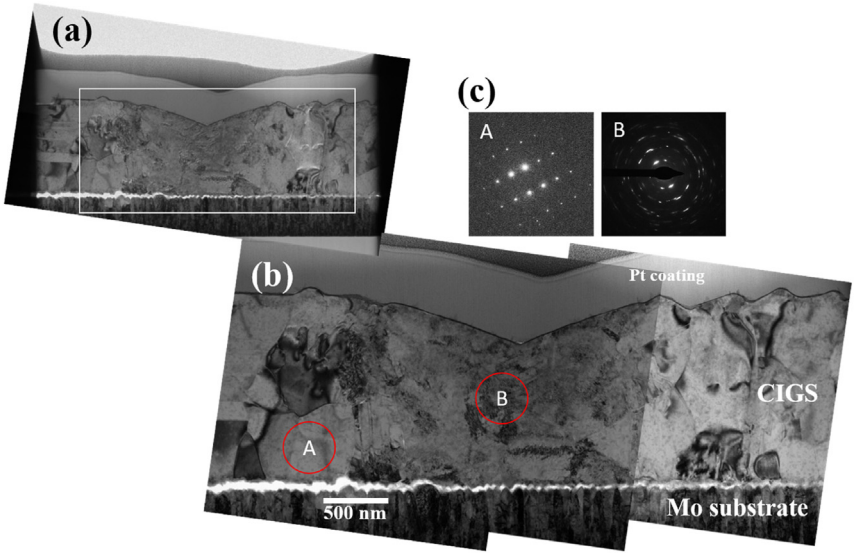

Fig. 4 – TEM images of the CIGS films after the nanoindentation tests at a depth of 500 nm. (a) indents on the CIGS microstructure; (b) enlarged micrograph of (a); (c) the electron diffraction patterns of circles A and B in Fig. 4b.

energy absorption in the films, and the bulge of the films might occur out-of-plane as shown in Fig. S4.

Figure 4 shows the TEM image of the sample when a load close to or less than the crack initiation load was applied. Figure 4 is a high-resolution image of the TEM sample shown in Fig. 1c. Figure 4b shows an enlarged image of the square in Fig. 4a. Cracks are not observed around the indents, and as shown in Fig. 2, no clear grain boundaries are visible under the indents. Figure 4c shows the electron diffraction patterns of circles A and B in Fig. 4b. Circle A is the part that was not affected by the indentation, and circle B is the part directly under the indentation and was externally stressed. As shown in the diffraction pattern, circle A exhibits the shape of a single crystal, whereas circle B part exhibits a mixed form of single crystal and polycrystalline. This indicates that the crystals of the CIGS films were deformed by external stress and new crystals were formed. In addition, a grain-subdivision phenomenon due to pressure was observed even in the specimen pressed to a depth of 1000 nm. Grain subdivision by pressure acted as a mechanism for absorbing energy. However, because of the brittleness of the CIGS films, the absorption of external energy by plastic deformation was limited, indicating that the energy was converted to fractures such as cracks.

The representative nanoindentation load–displacement (L–D) curves of the CIGS films are shown in Fig. 5. A pop-in phenomenon can be observed, as shown in Fig. S5, but it is not universal; however, the curve shown in Fig. 5a is representative. The slope of loading curve changes in the area indicated by the arrow in Fig. 5a. It is known that the pop-in phenomenon shown in Fig. S5 is generally closely related to the elastic–plastic transition caused by the dislocation movement. However, the results obtained herein indicate that the CIGS films are brittle compound semiconductor films, suggesting that the pop-in phenomenon has a deeper relationship with the crack of the films than with the elastic–plastic transition.

Based on the findings of Bei et al. [5] and Morris et al. [6], a loading equation based on the elastic behavior was used, and

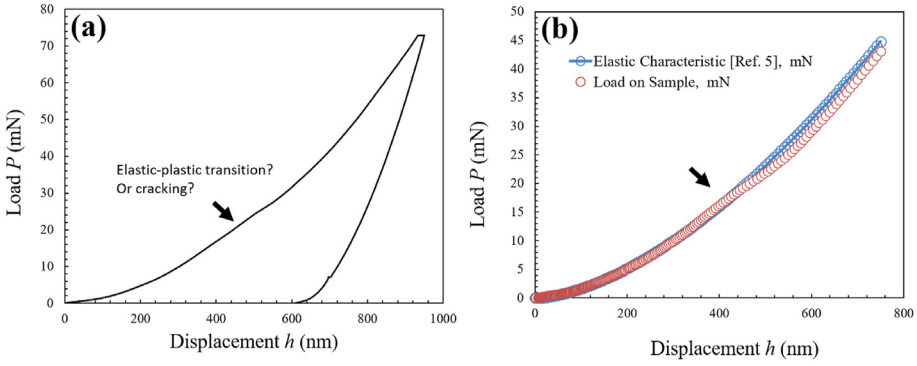

Fig. 5 – Nanoindentation results of the co-sputtered CIGS films: (a) representative load–displacement (L–D) curve when load was applied to a depth of 60% of the films; (b) and (c) comparison of the experimental results and the elastic characteristic curve obtained based on ref (Ref. [5]) deviated after approximately 500 nm indentation depth (b) and deviated early stage of loading.

the exponent term was set to 1.69. In this study, when the exponent was set to 1.69, it showed no fitting when applied to the elastic section where cracks did not occur. This could be attributed to the slightly different condition of the samples compared to those of existing studies such as curvature. Therefore, in this study, the exponent term was set to 1.633, and it was determined that the elastic section and load curve after cracking were more reasonable. Figure 5b is a superimposed graph of the completely elastic behavior based on the research of Bei et al. [5]. As shown in the image, the difference from the actual experimental curve occurs at the arrow portion indicated in Fig. 5a, i.e., at a depth of 400–500 nm and load of 20–25 mN. In addition, Fig. S6a shows a case wherein the load received from the initial stage of loading was lower than that of the elastic behavior is observed. Whereas, Fig. S6b shows a case wherein the load in the elastic characteristic curve is lower than the actual test load. Particularly, there was a slight difference in the mechanical behavior of the films with and without the application of CSM, and research on this is currently ongoing. Figure 6 shows the actual experimental and calculated *L–D* curves of the films when pressed to a depth of 500 nm. The phenomena shown in Fig. 5 were not observed, and the overall properties of the films were almost elastic. In addition, all the dozens of indentation experiments showed almost similar results. This is believed to be due to the fact that the P_{max} was almost 20 mN and the external stress applied was not sufficient to induce cracks, as discussed in the previous SEM and TEM analysis. These results indicate that the CIGS films fabricated herein can withstand external stress up to a local stress environment of approximately 25 mN without cracking. In the study of Gerthoffer et al. [1], the depth and load of crack formation were reported to be approximately 600 nm and 25 mN, respectively, which are similar to those obtained herein.

The elastic modulus and hardness of the CIGS films on the Mo/SLG substrate were measured based on the average values at indentation depth from 200 to 400 nm. To avoid uncertainties in the contact surface due to surface roughness, the minimum depth was estimated as 200 nm based on the measured data (shown in Fig. S3) and the maximum depth was estimated as 400 nm because we assumed that a force of 25 mN almost completely penetrated an indentation depth of 400 nm. Therefore, the elastic modulus of the films indented to a depth of 500 nm without cracks was selected as the elastic modulus of the CIGS films used in this study. The elastic modulus decreased with an increase in the indentation depth. This is because the films were not densely formed or were not completely adhered to the substrate. The elastic modulus and hardness of the CIGS films on the Mo substrate were approximately 88.5 ± 2.2 and 5.89 ± 0.23 GPa, respectively. These values are slightly higher than the results of Gerthoffer et al. [1], but similar to those of Lai et al. [3]. The slight differences could be attributed to the difference in the fabrication process, chemical composition, and type of substrate, among others. Thus, the results of this study are consistent with those of existing literature.

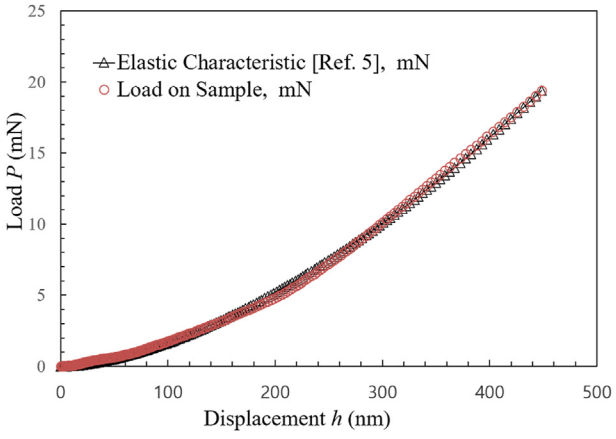

Fig. 6 – Nanoindentation results loaded at an indentation depth of 30% of the thickness of a CIGS films fabricated by co-sputtering method. Comparison of the experimental results and the elastic characteristic curve obtained based on (Ref. [5]).

4. Conclusions

The mechanical behavior of Cu(In,Ga)Se_2 (CIGS) light-absorbing films synthesized by co-sputtering method on soda-lime glass (Mo/SLG) substrates was investigated by nanoindentation. The transmission electron microscopy (TEM) analysis revealed that the CIGS films fabricated herein was well formed with large grains (more than 1 μm), indicating that it is suitable for application as a light-absorbing layer. The mechanical behavior of the films was continuously observed under various indentation depth using a nanoindenter™ in the continuous stiffness measurement (CSM) mode. To measure the mechanical properties of the CIGS film, maximum loads of 20 and 70 mN were applied to the CIGS films with a nanoindenter, and the mechanical properties were measured to a depth of 500 and 1000 nm, respectively. The comparison of the *L–D* curve based on the theoretical elastic films, considering the curvature of the indenter tip and the *L–D* curve obtained from the actual experiment, revealed that the CIGS films cracked under an indentation load of approximately 25 mN. Therefore, the Young's modulus and hardness of the CIGS films were measured using the sample subjected to pressure cracking, and were approximately 88.5 ± 2.2 GPa and 5.89 ± 0.23, respectively. These values are similar or slightly higher than those of the existing literature, and the error range could be attributed to the differences in the microstructure, manufacturing process, and chemical composition of the films. The TEM images revealed that most of the cracks were intergranular fractures, while some were intragranular fractures. The fracture toughness (K_C) of the CIGS films was calculated to be approximately 0.22 MPa$\sqrt{m}$, indicating that the CIGS films were very brittle, which is similar to soda-lime glass.

The indentation pressure caused grain-subdivision or refinement, which eventually led to the cracking of the entire thickness of the thin film when the pressure exceeded 25 mN. To manufacture films suitable for application in flexible electronic devices, the films should be capable of efficiently absorbing external stress. Therefore, it is important to develop a mechanism to improve the adhesion of grain boundaries and to efficiently generate grain subdivision. In addition, it is

important to develop materials that can absorb external stress, while maintaining its electrical properties. Research is underway with the possibility that 2D materials may exhibit these properties.

In the case of the films, it should be noted that the fracture toughness measurement is not easy to interpret due to the influence of the substrate, and the indentation-based method may have errors [27]. Nevertheless, it must be a useful method because the properties of the fracture toughness of the films can be measured relatively easily.

Declaration of Competing Interest

The authors declare that they have no known competing financial interests or personal relationships that could have appeared to influence the work reported in this paper.

Acknowledgements

This research was funded by 1) the Basic Science Research Program through the National Research Foundation of Korea (NRF) funded by the Ministry of Education (No. 2018R1D1A1B07041358); 2) the National Research Foundation of Korea (NRF) grant funded by the Korean Government (MISP) (No. NRF-2018R1A5A1025594); 3) the National Research Foundation of Korea (NRF) grant funded by the Korea government (MSIT) (No. 2020R1A2C2007590).

Appendix A. Supplementary data

Supplementary data to this article can be found online at https://doi.org/10.1016/j.jmrt.2021.05.059.

REFERENCES

[1] Gerthoffer A, Poulain C, Roux F, Emieux F, Grenet L, Perraud S. CIGS solar cells on ultra-thin glass substrates: determination of mechanical properties by nanoindentation and application to bending-induced strain calculation. Sol Energy Mater Sol Cells 2017;166:254–61.
[2] Green MA, Emery K, Hishikawa Y, Warta W, Dunlop ED. Solar cell efficiency tables (version 47). Prog Photovoltaics Res Appl 2016;24:3–11.
[3] Lai TY, Hsiao YJ, Fang TH. Mechanical properties of CIGS film with different metallic composition by co-evaporation method. Mater Res Express 2017;4:115006.
[4] Dukino RD, Swain MV. Comparative measurement of indentation fracture toughness with Berkovich and Vickers indenters. J Am Ceram Soc 1992;75:3299–304.
[5] Bei H, George EP, Hay JL, Pharr GM. Influence of indenter tip geometry on elastic deformation during nanoindentation. Phys Rev Lett 2005;95:045501.
[6] Morris JR, Bei H, Pharr GM, George EP. Size effects and stochastic behavior of nanoindentation pop in. Phys Rev Lett 2011;106:165502.
[7] Assmann L, Bernede JC, Drici A, Amory C, Halgand E, Morsli M. Study of the Mo thin films and Mo/CIGS interface properties. Appl Surf Sci 2005;246:159–66.
[8] Koo B, Nam S, Haight R, Kim S, Oh S, Cho M, et al. Tailoring photoelectrochemical performance and stability of Cu(In,Ga)Se_2 photocathode via TiO_2-coupled buffer layers. ACS Appl Mater Interfaces 2017;9:5279–87.
[9] Koo B, Kim D, Boonmongkolras P, Pae SR, Byun S, Kim J, et al. Unassisted water splitting exceeding 9% solar-to-hydrogen conversion efficiency by Cu(In,Ga)$(S,Se)_2$ photocathode with modified surface band structure and halide perovskite solar cell. ACS Appl Energy Mater 2020;3:2296–303.
[10] Nanoindenter G200 Specifications. KLA, Inc.; 2012.
[11] Lucas BN, Oliver WC. Indentation power-law creep of high-purity indium. Metall Mater Trans 1999;30:601–10.
[12] Oliver WC, Pharr GM. Measurement of hardness and elastic modulus by instrumented indentation: advances in understanding and refinements to methodology. J Mater Res 2004;19:3–20.
[13] Lawn BR, Wilshaw TR. Indentation fracture: principles and applications. J Mater Sci 1975;10:1049–81.
[14] Evans AG, Charles EA. Fracture toughness determination by indentation. J Am Ceram Soc 1979;59:371–2.
[15] Sebastiani M, Johanns KE, Herbert EG, Pharr GM. Measurement of fracture toughness by nanoindentation methods: recent advances and future challenges. Curr Opin Solid State Mater Sci 2015;19(6):324–33.
[16] Ghosh G. Elastic properties, hardness, and indentation fracture toughness of intermetallics relevant to electronic packaging. J Mater Res 2004;19:1439–54.
[17] Dukino RD, Swain MV. Comparative measurement of indentation fracture toughness with Berkovich and Vickers indenters. J Am Ceram Soc 1992;75:3299–304.
[18] Doerner MF, Nix WD. A method for interpreting the data from depth-sensing indentation instruments. J Mater Res 1986;1:601–9.
[19] Oliver WC, Pharr GM. An improved technique for determining hardness and elastic modulus using load and displacement sensing indentation experiments. J Mater Res 1992;7:1564–83.
[20] Sneddon IN. The relation between load and penetration in the axisymmetric boussinesq problem for a punch of arbitrary profile. Int J Eng Sci 1965;3:47–57.
[21] Kuhn H, Medlin D. ASM International, Member/Customer Service Center. 2000. Materials Park; OH 44073-0002; USA.
[22] Park K, Park J, Park S, Lee D, Yoo D, Shin S, et al. Fabrication of Cd-free $CuInSe_2$ solar cells by wet-process. J Mater Sci 2017;52(23):13533–40.
[23] Cook RF, Pharr GM. Direct observation and analysis of indentation cracking in glasses and ceramics. J Am Ceram Soc 1990;73:787–819.
[24] Chen J. Indentation-based methods to assess fracture toughness for thin coatings. J Phys D Appl Phys 2012;45:203001.
[25] Anstis GR, Chantikul P, Lawn BR, Marshall DB. A critical evaluation of indentation techniques for measuring fracture toughness: I, direct crack measurements. J Am Ceram Soc 2006;64:533–8.
[26] Jun H, Kim Y, Lee SJ, Kang N, Kim K, Kim M, et al. Anomalous multiple pop-in behavior in Cu–Sn-based intermetallic compounds during nanoindentation. Mater Sci Eng A 2014;612:192–6.
[27] Sebastiani M, Johanns KE, Herbert EG, Carassiti F, Pharr GM. A novel pillar indentation splitting test for measuring fracture toughness of thin ceramic coatings. Philos Mag A 2015;95:1928–44.